Entropy increase in confined free expansions via molecular dynamics and smooth-particle applied mechanics

Wm. G. Hoover

Department of Applied Science, University of California at Davis/Livermore and Lawrence Livermore National Laboratory, Livermore, California 94551-7808

H. A. Posch

Institut für Experimentalphysik, Universität Wien, Boltzmanngasse 5, A-1090 Wien, Austria

The eventual entropy increase of an ideal gas undergoing free expansion, $\Delta S = k \ln(V_{fin}/V_0)$, requires a "coarse-grained" hydrodynamic description because Gibbs' fine-grained entropy is unchanged in such a process. Smooth particle applied mechanics (SPAM) is well suited to the simulation and study of such problems because the particles in SPAM simulations can be of any size, from microscopic to macroscopic. SPAM furnishes a natural interpolation, or bridge, linking microscopic molecular dynamics to macroscopic continuum mechanics. We analyze particle-based simulations of ideal-gas free expansions from both the microscopic and the macroscopic points of view, comparing several dynamical estimates for the time development of the system entropy. Most of the entropy increase occurs rapidly, within a single sound traversal time. A local comoving version of turbulent hydrodynamics provides the most useful viewpoint for describing flows of this kind. [S1063-651X(99)07402-4]

I. FREE EXPANSIONS AND ENTROPY

The "confined free expansion," which results when a pressurized fluid is first exposed to a vacuum, and then confined by a box, is the prototypical irreversible isoenergetic process. During the free expansion and the subsequent equilibration there is no heat exchange with the system's surroundings and no work is done, establishing that the expansion process is adiabatic and isoenergetic: $\Delta E = \Delta Q - \Delta W \equiv 0$. The initial expansion phase is also nearly isentropic, with the gas cooling as it expands. Over 100 years ago, Boltzmann described such expansion processes, emphasizing that entropy is not generated until the directed motion of expansion is converted to the disordered motion we call heat [1].

Once the system reaches the walls confining it, so that the kinetic energy associated with the expansion can be converted to "heat," an entropy increase occurs. The details of this increase are what interest us here. We study the expansion of a "perfect" or "ideal" gas, with no explicit dissipation. Nevertheless, within the system the turbulent decays of the macroscopic velocity and temperature gradients give rise to an increasing thermodynamic entropy. With confining external boundary conditions, which ultimately bring the expansion to a halt, there eventually results an undoubted change of state, with a consequent increased entropy. The details of the macroscopic turbulent conversion of orderly motion into heat are complex and hard to treat theoretically.

Such an irreversible entropy increase is likewise difficult to understand at the microscopic level. When Hamiltonian mechanics generates the motion of the individual fluid particles, there can be no change in the system's fine-grained Gibbs' entropy. This follows from the constancy of the phase-space probability density f, according to Liouville's theorem [2]:

$$\dot{f} \equiv 0 \rightarrow \dot{S}_G \equiv -k(d/dt)\langle \ln f \rangle = -k \int \dot{f} \ln f \, d\Gamma \equiv 0.$$

These difficulties in accounting for increases in entropy using conventional macroscopic fluid mechanics or microscopic statistical mechanics are well-known, currently under active investigation by researchers in macroscopic turbulence and microscopic irreversible flows [3,4], and served to motivate our interest in exploring accurate numerical solutions of this problem.

Macroscopic hydrodynamics provides a quantitative estimate for the irreversible rate of entropy production in terms of the shear and bulk viscosities, (η, η_V), and the heat conductivity κ. Unless the temperature and velocity gradients are too large, the conversion of temperature and velocity differences into "heat," or internal energy, can be described by Newtonian viscosity and linear Fourier heat conductivity. If we ignore the bulk viscosity (which is appropriate for a monatomic ideal gas) and additionally assume that the two remaining transport coefficients are state independent, the local density of the irreversible entropy production from Newton's and Fourier's linear transport laws becomes

$$\dot{s} = (\eta/T)\dot{\epsilon}^2 + (\kappa/T^2)|\nabla T|^2,$$

where $\dot{\epsilon}$ is an effective shear strain rate. In two dimensions, with the local velocity components $\dot{x} = u$ and $\dot{y} = v$, the corresponding effective shear strain rate is given by

$$\dot{\epsilon}^2 \equiv (u_x - v_y)^2 + (u_y + v_x)^2.$$

From a more simplified point of view one might expect that most of the entropy increase would occur locally and discontinuously, through a complex pattern of interacting shock

and rarefaction waves which converts most of the kinetic energy of the developing flow directly into heat.

Because the confined free-expansion problem provides the simplest illustration of the paradoxical properties of Gibbs' entropy, and can be simulated by a variety of techniques relatively easily, we have chosen to explore it here. We use a robust and flexible numerical method which provides simultaneous insight into both the microscopic and macroscopic points of view, namely smooth particle applied mechanics (SPAM). In the case of a special two-dimensional monatomic ideal gas, this macroscopic method for solving the field equations of continuum mechanics turns out to be equivalent to ordinary microscopic molecular dynamics [5]. This link between the microscopic and macroscopic viewpoints is described further in Sec. II. In Secs. III and IV, we describe the details of the macroscopic simulations, and the results. Our conclusions make up Sec. V.

II. THE SMOOTH-PARTICLE DESCRIPTION OF AN IDEAL GAS

Smooth-particle solution techniques, as developed by Lucy and Monaghan in 1977 [6,7] and applied more recently to a variety of problems in fluid and solid mechanics [8–10], can be used to solve the continuum equations in a simple, and stable, way. In this approach the smooth particles, each with a mass m, and with individual velocities $\{v_i\}$ and internal energies $\{me_i\}$, move according to equations of motion which contain in them the macroscopic equation of state:

$$\left\{ m\ddot{r}_i \equiv m\dot{v}_i = -m^2 \sum_j \; [(P/\rho^2)_i + (P/\rho^2)_j] \cdot \nabla_i w_{ij} \right\}.$$

Here P is the pressure tensor and $w_{ij} = w(r_{ij})$ is the smooth-particle "weight function," which describes the spatial influence of each particle on its surroundings. The range of w—typically a few interparticle spacings—is conventionally denoted h. If the pressure is purely hydrostatic, without shear contributions, as in the two-dimensional ideal gas of interest here (with $E = PV = NkT$), the smooth-particle equations of motion give central forces, with the $\{ij\}$ pair contributions parallel to the corresponding interparticle separation vectors $\{r_{ij}\}$. The equilibrium hydrostatic equation of state modulates the pair interaction. The densities of the N particles making up the system, $\{\rho_i\}$, are the summed-up contributions from all particles within the range h of the smooth-particle weighting function $w(r):\{\rho_i \equiv m\Sigma_j w(r_{ij})\}$. The largest contribution to each particle's density is its own "self contribution," $mw(0)$.

When the smooth-particle motion equations are multiplied by the corresponding particle velocities, and summed up, the result is the time-rate-of-change of the laboratory-frame kinetic energy K:

$$K = \sum_i \; mv_i\dot{v}_i = -m^2 \sum_i \sum_j \; [(P/\rho^2)_i + (P/\rho^2)_j] : (v\nabla)_i w_{ij}$$

$$= -(m^2/2) \sum_i \sum_j \; [(P/\rho^2)_i + (P/\rho^2)_j] : (v_i - v_j)\nabla_i w_{ij}.$$

From the macroscopic energy equation for an inviscid nonconducting gas, $\dot{e} = -(P/\rho)\nabla \cdot v$, where the pressure P is now a scalar, rather than a tensor, the smooth-particle equations for the time development of the individual particle internal energies are [6,7]

$$\left\{ m\dot{e}_i = (m^2/2) \sum_j \; [(P/\rho^2)_i + (P/\rho^2)_j](v_i - v_j) \cdot \nabla w_{ij} \right\}.$$

Here e_i is the internal energy per unit mass for particle i. Thus, in this special inviscid-gas case, the total energy $E + K = m\Sigma_i[e_i + (v_i^2/2)]$ is conserved exactly by the smooth-particle equations:

$$m\sum_i \; (\dot{e}_i + v_i\dot{v}_i) = (m^2/2) \sum_i \sum_j \; [(P/\rho^2)_i + (P/\rho^2)_j]$$
$$\times [(v_i - v_j) - (v_i - v_j)] \cdot \nabla_i w_{ij} \equiv 0.$$

The total internal energy E is the thermodynamic state energy, and excludes the additional kinetic energy K due to convective motions of the gas.

Note that the special polytropic equation of state, $P = (D^2/2m)\rho^2$, gives particle forces precisely equal to the negative gradients of a "weight potential" $W(\{r_{ij}\}) \equiv mD^2\Sigma_{i<j} w_{ij}(r_{ij})$. Thus, within an additive constant for each particle [the "self-contributions" $\phi(0) \equiv (mD^2/2)w_{ii}(0)$, which do not contribute to the accelerations], the smooth-particle density sums equal twice the corresponding individual smooth-particle internal energy sums, which in turn turn out to be exactly equivalent to each particle's share of the pairwise-additive interaction energies of Hamiltonian molecular dynamics: $\Phi = \Sigma_{i<j}\phi(r_{ij}) \equiv m\Sigma_i e_i$. The weighting function $w(r_{ij}) \equiv \phi(r_{ij})/mD^2$ here plays the role of a microscopic pair potential. Thus all of the individual macroscopic smooth-particle continuum trajectories are precisely "isomorphic" to corresponding microscopic particle trajectories calculated with molecular dynamics. The two approaches, macroscopic and microscopic, have identical solutions [5]. We have chosen the symbol D so as to emphasize the units of the arbitrary constant appearing in the isentropic equation of state. In two space dimensions D corresponds to a diffusion coefficient, the square of a length divided by a characteristic time. In three space dimensions the corresponding D would vary as the 5/2 power of a length, again divided by a characteristic time.

The microscopic pressure tensor follows from the virial theorem [11]. The expression which results,

$$PV \equiv P^K V + P^\Phi V = (1/m) \sum_i \; (pp)_i + \sum_{i<j} \; (rF)_{ij},$$

where $r_{ij} = r_i - r_j$ and F_{ij} is the force on particle i due to its interaction with particle j, can be evaluated using molecular dynamics. For a uniformly dense distribution of particles the sum over pairs of particles approaches an integral:

$$P^\Phi V \rightarrow (N/2) \int_0^\infty 2\pi r(N/V)rF(r)dr,$$

where N/V is the number density of the smooth particles. With the special hydrostatic macroscopic ideal-gas equation of state, $P \equiv (D^2/2m)\rho^2$, the same integral results, but with the interparticle force F replaced by $-mD^2\nabla w$. From the normalization of the weight-function integral,

$$\int_0^\infty 2\pi r w \, dr \equiv \int_0^\infty -\pi r^2 w' \, dr \equiv 1,$$

the uniform-density limit of the microscopic potential pressure, P^Φ, reproduces the complete macroscopic equation of state, $P = (D^2/2m)\rho^2$. The remaining kinetic portion of the microscopic pressure tensor, P^K, corresponds, in the macroscopic hydrodynamic interpretation, to a local turbulent Reynolds stress, $-\sigma_{\mathrm{Reynolds}} \equiv \rho[\langle vv \rangle - \langle v \rangle \langle v \rangle]$ [12].

Apart from an additive constant, the macroscopic ideal-gas entropy is $Nk \ln[(V/N)(E/N)]$. We will see that solutions of the inviscid nonconducting Euler equations for the motion of such a gas require an additional turbulent correction, based on local velocity fluctuations, to the internal energy used in this entropy formula. The macroscopic entropy is quite different from that following from Gibbs' statistical mechanics. In Gibbs' approach, where the potential energy of the underlying smooth-particle fluid is essentially constant, Gibbs entropy is $Nk \ln[(V/N)(K/N)]$, and thus lies below the macroscopic entropy by $Nk \ln(E/K)$. Though this entropy difference does not affect the systematic macroscopic dynamics at all, it does affect fluctuations, as well as recurrence probabilities, in interesting ways, as is discussed further below.

The smooth-particle solutions necessarily approach those of continuum mechanics as the number of particles is increased. To approach this limit computationally, it is necessary that the range of the weight function be sufficiently large, so that fluctuations can be ignored and, simultaneously, sufficiently small that surface effects can be ignored. We have explored both these effects in simulating the free expansion of a two-dimensional ideal-gas represented by smooth particles.

III. MACROSCOPIC SIMULATIONS OF FREE EXPANSION USING SPAM

With SPAM, a solution of the partial differential field equations of continuum mechanics,

$$\{\dot{\rho}/\rho = -\nabla \cdot v; \rho\dot{v} = -\nabla \cdot P; \rho\dot{e} = -\nabla v : P - \nabla \cdot Q\},$$

reduces to the solution of a set of ordinary differential equations for the particle motions and energies, with interparticle forces derived from the weight functions $\{w_{ij}(r_{ij})\}$ and the macroscopic equation of state. In the special ideal-gas case we consider here, viscosity and heat conduction are both absent, so that the heat flux Q vanishes and the pressure is hydrostatic, with $P_{xx} = P_{yy} = P = \rho e = (D^2/2m)\rho^2$. The macroscopic energy equation is automatically satisfied in this case, so that the $\{\dot{e}_i\}$ equations need not be solved explicitly. Exploratory simulations, with an assortment of boundary conditions and weight functions, led us to choose Lucy's weight function [6], with the range h large enough, h

$= 6\sqrt{m/\rho_0}$, to include several particles, even at the final minimum value of the density, $\rho_{\mathrm{fin}} = \rho_0/4$:

$$w_{\mathrm{Lucy}}(r < h) \equiv (5/\pi h^2)[1 + 3(r/h)][1 - (r/h)]^3;$$

$$\int_0^h 2\pi r w(r) dr \equiv 1.$$

The two-dimensional normalization condition determines the multiplicative constant $(5/\pi h^2)$. The mass, length, and time scales are given by the particle mass m, the initial square-lattice spacing $\sqrt{m/\rho_0}$, and $m/(D\rho_0)$, respectively.

We simulate a macroscopic free expansion by removing the four rigid reflecting walls defining an $L \times L$ box. We simultaneously impose (i) periodic boundaries with a doubled sidelength $2L$, so that the volume (area) increases instantaneously, at constant energy, by a factor 4, and (ii) small random particle velocities, with zero sum, chosen so that the initial energy per particle is exactly equal to the large-system static limit, $E/N = \rho_0 D^2/2$. The kinetic energy compensates for the small missing "surface energy" of those particles close to the boundary of the initial rigid $L \times L$ box. The large-N number of pairs of interacting particles, for $\sqrt{N/V_0} = 6/h$, decreases from about $60N$ to about $15N$ during the evolution toward the lower-density final state. Provided that the final state has uniform density, $\rho_0/4$, conservation of energy predicts an increase in per-particle kinetic energy of $3\rho_0 D^2/8$. From the thermodynamic standpoint we would also hope to find a corresponding entropy increase of $k \ln 4$ per particle, when the kinetic energy associated with the irreversible expansion has finally been converted into heat. In the absence of any explicit dissipative transport in the gas we expect the characteristic time for the effective dissipation to be of the order of the sound traversal time, $2L/c$. We investigate this expectation, and the sensitivity of the decay to the number of smooth particles, in the following section.

IV. SIMULATIONS AND RESULTS

For simplicity, we begin with a square lattice of initial particle coordinates, with the lattice spacing of $\sqrt{m/\rho_0} = \sqrt{V_0/N} \equiv 1$ setting the distance scale. We choose the particle mass $m \equiv 1$ and the constitutive constant $D \equiv 1$ to set the corresponding mass and time scales in the numerical work. In order to quantify surface effects, it is convenient to consider the series of simulations $\sqrt{N} = 2^n; 4 \leqslant n \leqslant 8$. Although it is possible to equilibrate the systems initially, either at constant energy or at constant kinetic temperature, and with either rigid or periodic boundaries, results for our simpler initial conditions are in no way essentially different from those other possibilities. We also implemented hexagonal periodic boundaries and carried out a series of fourfold expansions. The resulting time histories were very similar to those obtained with the slightly simpler square geometry.

We solved the smooth-particle equations of motion with an accurate fourth-order Runge-Kutta integrator. Time steps of $0.02m/(\rho_0 D)$, or even $0.05m/(\rho_0 D)$, are sufficiently small for accurate trajectories, as judged by reversing the motion over several hundred time steps. Larger systems could be simulated relatively easily, on parallel machines,
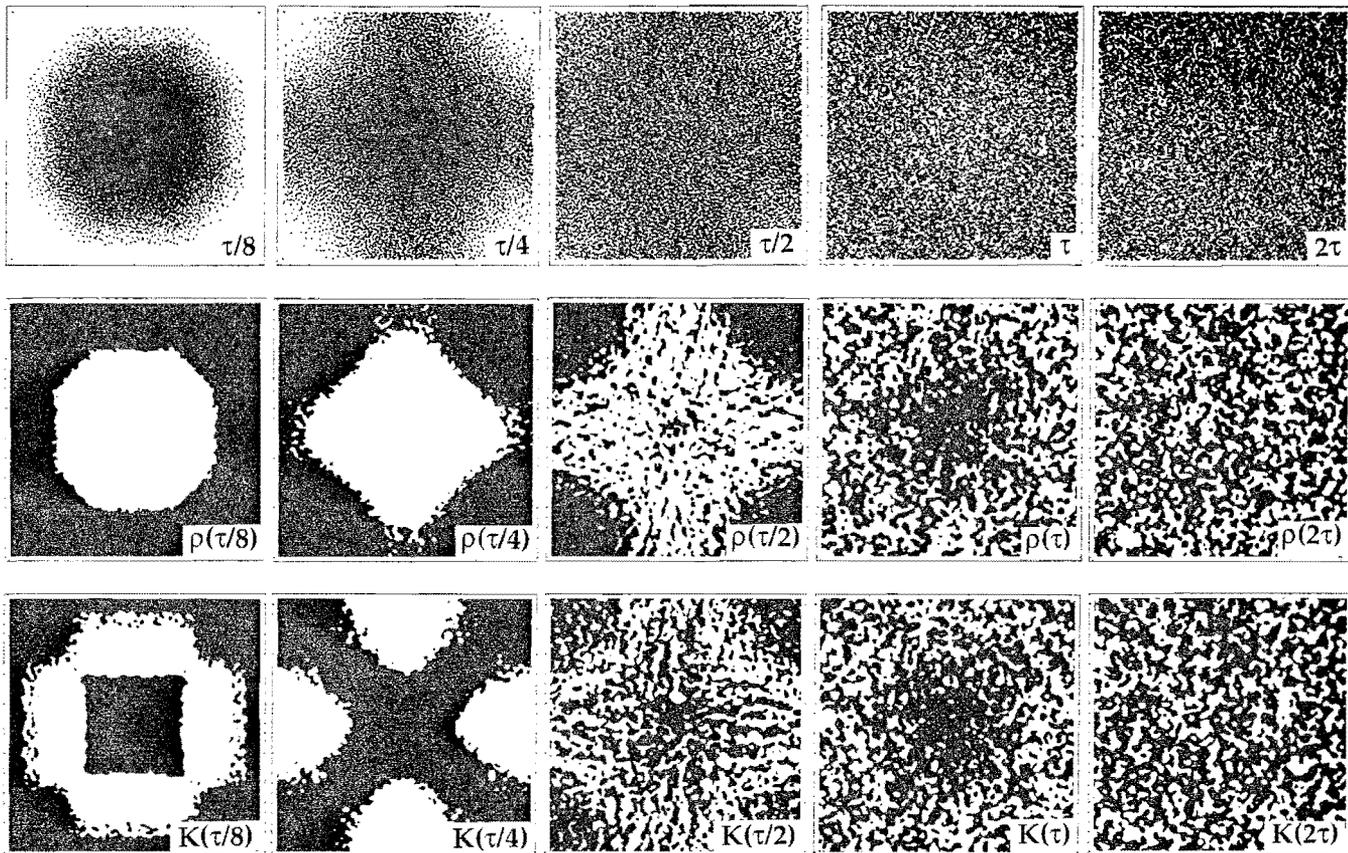
FIG. 1. Snapshots of a 16 384-particle simulation of the fourfold expansion of an ideal gas, using Lucy's weighting function with h $6\sqrt{m/\rho_0}$. The individual particle locations, as well as grid-based contour representations of the density and kinetic energy, relative to the mean flow, are shown at times, relative to the sound traversal time, of $\{1/8, 1/4, 1/2, 1, 2\}$. In the contour plots the white regions have above-average density (middle row) or kinetic energy (bottom row) while the black regions lie below the corresponding averages.

but the details are already sufficiently clear with the 65 536-particle simulations possible on a serial machine. During each simulation, we monitored the positions, internal and convective energies, and the corresponding entropies of the particles, as is discussed below.

Figure 1 shows a series of snapshots of particle positions from a typical simulation, with 16 384 particles. Because the smooth-particle method makes it easy to calculate all the field variables on a regular grid,

$$\begin{cases} \rho_g \equiv m \sum_i w_{ig} : (\rho v)_g \equiv m \sum_i v_i w_{ig} ; \\ (\rho v v)_g \equiv m \sum_i v_i v_i w_{ig}, \end{cases}$$

we include also in the figure grid-based contour plots of the density and the kinetic energy, relative to the mean flow, as the flow develops.

Initially, as suggested by an energy-conservation principle resembling Bernoulli's [13] [which states that the energy e $+(P/\rho)+(1/2)v^2$ is conserved along streamlines], four planar rarefaction fans move out, perpendicular to the walls of a confining $2L \times 2L$ chamber, with a maximum velocity a bit larger than the sound velocity c, and consistent with the principle

$$m v_{max}^2 / 2 = m[e + (P/\rho)] \equiv 2me \rightarrow v_{max} = 2\sqrt{P/\rho} = \sqrt{2}c.$$

The directed kinetic energy generated by the expansion into vacuum is soon "dissipated," or converted, into quite irregular shorter-wavelength disturbances, by the collisions of pairs of periodically repeated rarefaction fans. The time required for this energy conversion, at least on a visual level, is very brief, less than a sound traversal time. Because this feature of the solutions is common to all the system sizes that we could investigate, we conclude that it represents the "true" solution as well, to the extent that Lyapunov-unstable (due to turbulence) continuum equations have "solutions." True viscous and conductive dissipative transport is only effective at much longer times, of order L^2/D rather than L/c.

SPAM, like other grid-based numerical schemes, automatically includes an intrinsic shear viscosity [14] (as well as a related heat conductivity [15]) which depends upon the number of particles used to describe the flow. In simulations for which the kinetic energy allows relatively soft interpenetrating collisions to occur, Enskog's high-density kinetic theory can be used to estimate the intrinsic viscosity, with the result [15,16]

$$\eta_{intrinsic} = (\sqrt{mkT}/h)(kTh^2/mD^2)^2.$$

We carried out isoenergetic simulations of the shear viscosity over a range of strain rates, $\dot{\epsilon} \equiv du_x/dy$, using the methods of Ref. [14]. The results are given in Table I, and are, for the lower strain rates, a bit larger than the Enskog estimate,

TABLE I. Shear viscosity $\eta \equiv -P_{xy}/\dot{\epsilon}$ for the Lucy potential with $h = 6\sqrt{m/\rho_0}$ and $\rho/\rho_0 = 1/4$. The data were obtained using 1024 particles with a total energy of $(N/2)D^2\rho_0 = 512D^2\rho_0$ and a time step $0.005m/(D\rho_0)$. The total simulation time is τ, of which the last half was used for determining the viscosity and pressure tensor. The components of the pressure tensor are shown as the sums of kinetic and potential contributions. Simulations at reduced strain rates of 0.001 and 0.002 indicate instabilities of the type discussed in Ref. [14].

$\tau D\rho_0/m$	$\dot{\epsilon}m/(D/\rho_0)$	$\eta/(D\rho 0)$	$(P_{xx}V/N)D^2\rho_0$	$(P_{xy}V/N)D^2\rho_0$	$(P_{yy}V/N)D^2\rho_0$
200000	0.0001	28.5	0.3586+0.1225	−0.0114+0.0000	0.3582+0.1225
86500	0.0002	27	0.3618+0.1225	−0.0212+0.0001	0.3551+0.1225
18000	0.0004	29	0.3763+0.1224	−0.0472+0.0001	0.3410+0.1224
20000	0.0005	29	0.4005+0.1223	−0.0582+0.0001	0.3174+0.1223
180000	0.0050	7.99	0.5161+0.1217	−0.1606+0.0007	0.2032+0.1226
70000	0.0100	4.356	0.5547+0.1214	−0.1750+0.0008	0.1641+0.1231
30000	0.0200	2.094	0.5993+0.1211	−0.1684+0.0009	0.1196+0.1236
80000	0.0500	0.720	0.6461+0.1208	−0.1447+0.0008	0.0730+0.1242
30000	0.1000	0.307	0.6706+0.1207	−0.1234+0.0006	0.0486+0.1246

$\eta = 19D\rho_0$. The agreement is similar to that found previously, at a lower temperature, in Ref. [14].

The present viscosity data differ from those of Ref. [14] in two ways. First, we are including the self-interaction, $mD^2w(0)/2$, in the per-particle energies here. These were omitted in Ref. [14]. The increased energy here, about 4%, is of little consequence. The densities, energies, and strain rates in the present work are in corresponding states with higher densities, energies, shear viscosities, and strain rates, all of which are increased by a common scale factor. Thus the Enskog shear viscosity, here $19D\rho_0$ at $\rho = \rho_0/4$ and $kT = 0.375D^2\rho_0$, must be increased by a factor 4, to $76D\rho_0$, in order to describe a corresponding sheared system at $\rho = \rho_0$ and $kT = 1.5D^2\rho_0$, with a strain rate four times greater. Taking this correspondence into account, the data of Table I are nicely consistent with the relatively-lower-energy data compiled in Ref. [14]. In Fig. 2 we show all the viscosity data, from both sources, all expressed in units consistent with those of Ref. [14].

Increasing $N \propto L \times L$, the number of smooth particles representing a particular macroscopic flow, with fixed values of the SPAM simulation parameters, h, m, and D, causes the effective Reynolds number of the flow to increase as $N^{1/2}$, because the Reynolds number is proportional to the box size L. Over the range of sizes examined here, there was no indication of a slowing of the dissipation with increasing box
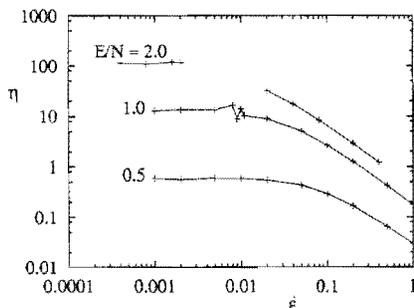
size. In fact, the main entropy increase appears to occur in approximately one sound-traversal time, independent of system size. Very long simulations show only fluctuations at long times, with no tendency for a further systematic entropy increase.

The simplest description of the ideal-gas equilibrium entropy, $S \equiv Nk \ln(e/\rho)$, is worthless for this problem, because this entropy is necessarily a constant of the motion

$$me_i = (D^2/2)m\sum_j w_{ij} \equiv (D^2/2)\rho_i,$$

where we include the "self" w_{ii} term in the sum. Evidently the kinetic energy of the motion, which cannot be dissipated with inviscid motion equations, must be taken into account too. The simplest such "improvement," adding in the laboratory-frame kinetic energies of the particles, $\{mv_i^2/2\}$, provides a very substantial and wholly unrealistic [1] entropy increase during the early stages of expansion, where the motion is adiabatic and reversible, and well before the irreversible interaction of the expanding rarefaction fans takes place. See Fig. 3 for typical time histories of Eulerian "laboratory-frame" entropies for a variety of system sizes:

$$S_{lab} \equiv k\sum_i \ln\{[e_i + (v_i^2/2)]/\rho_i\}.$$

Evidently this lab-frame entropy already begins to increase during the earliest stage of the flow, when only nearly-isentropic rarefaction fans are present.

To avoid the unrealistic, premature entropy increase shown in these laboratory-frame entropies, it is evident that the kinetic energies at the locations of the continuum particles, $\{m\langle v^2\rangle/2\}$, need to be measured relative to the co-moving "Lagrangian" frames at the particle locations. The local kinetic energies of the mean motion, $\{m\langle v\rangle^2/2\}$, cannot contribute to the thermodynamic entropy. Making this subtraction leads to the corresponding "Lagrangian" entropy, shown also in Fig. 3,

$$S_{Lag} = k\sum_i \ln\{[e_i + (1/2)\langle(v - \langle v\rangle_i)^2\rangle_i]/\rho_i\}.$$

FIG. 2. Shear viscosity $\eta \equiv -P_{xy}/\dot{\epsilon}$ for the Lucy potential with $h = 3\sqrt{m/\rho_0}$ and $\rho = \rho_0$. In order to make the present data comparable to those of Ref. [14], the strain rate and the shear viscosity from Table I, for $h = 6\sqrt{m/\rho_0}$, have both been increased, by a factor 4.
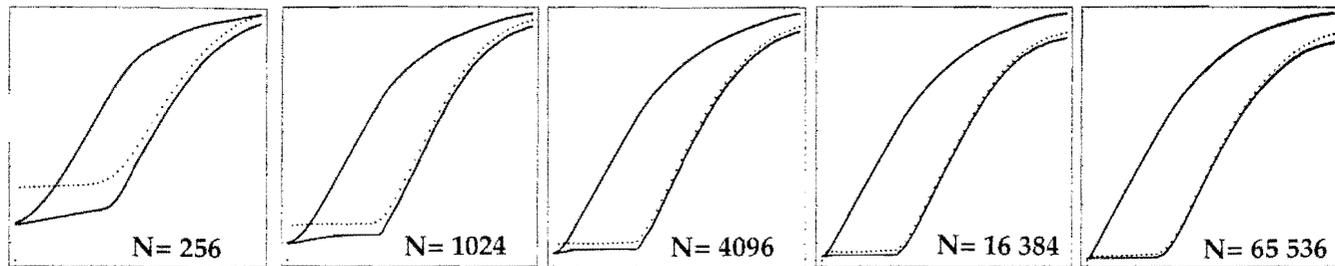
FIG. 3. Time-development of the "laboratory-frame" entropy (upper curve), the Lagrangian entropy (lower curve), and the grid-based entropy (dots), for systems of 256, 1024, 4096, 16 384, and 65 536 particles. The time scales show one-half sound traversal time in each case. The entropy range shown is $Nk \ln 4$ in each case.

The comoving Lagrangian picture of fluid properties is equivalent to making the assumption of local thermodynamic equilibrium. As Boltzmann pointed out [1], the corresponding Lagrangian entropy increase is delayed until the rarefaction fans collide with their "container"—here represented by periodic images of the original system.

An alternative version of the comoving entropies, using a fixed grid rather than the grid made up of moving particles, can be based on smooth-particle entropies evaluated at the fixed grid points:

$$S_{\text{grid}} = -(k/m) \int_{-L}^{+L} \int_{-L}^{+L} \rho_g \ln\{[e_g + (1/2)(\langle v^2 \rangle_g$$

$$- \langle v \rangle_g^2)]/\rho_g\} dx \, dy.$$

ese entropies are also shown in Fig. 3, for five different system sizes. With systems of a few thousand particles there is excellent agreement between the grid-based and particle-based averages, as must be true for the validity of the smooth-particle approach. The main physical conclusion from these simulations is independent of the entropy representation: the coarse-grained entropy increase is substantially complete in a time of the order of the sound traversal time. Conventional transport processes, which could be included with a slight increase in computational expense, are not very important to this free-expansion process. Ordinary transport contributes only a relatively small amount of the irreversible entropy production.

The two-dimensional nature of our simulations appears to be somewhat artificial, at first glance. But it is interesting to note that our polytropic equation of state, with $\gamma \equiv C_P/C_V = 2$, corresponds exactly to the dynamics of shallow water, where the pressure and density are integrated through the thickness of a water film with a perpendicular gravitational field [17]. Simulations in two dimensions also reduce the influence of surface effects and facilitate visualization. There is no difficulty in carrying out analogous three-dimensional work. In the three-dimensional case it is most "natural" to imagine the continuum mechanics of a monatomic ideal gas with the polytropic isentrope $P \propto \rho^{5/3}$. The SPAM trajectories for this macroscopic equation of state are isomorphic to se following from the three-dimensional molecular dynics of a system with the embedded-atom potential Φ:

$$\Phi(\{r_i\}) \propto \sum_i \rho_i^{2/3} : \left\{ \rho_i \equiv m \sum_j w(r_{ij}) \right\}.$$

In this embedded-atom picture, $m \Sigma w$ represents an electronic density, into which the nuclei at coordinates $\{r_i\}$ are embedded [18].

V. CONCLUSION

The irreversible expansion of an ideal fluid can be described equally well at the microscopic level of molecular dynamics and at the macroscopic level of smooth-particle applied mechanics, despite the lack of any dissipative transport coefficients in the corresponding continuum model. Evidently the conversion of the energy of compression into heat occurs primarily through processes proceeding at the speed of sound, rather than through the much slower dissipative processes of shear viscosity and heat conduction. Provided that the local velocity fluctuations are included in the internal energy, the coarse-grained entropy increase described by irreversible thermodynamics is nicely, and simply, accounted for, and in a way which is insensitive to the number of particles used in the simulations.

We can use Gibbs' statistical probabilities to demonstrate an interesting property of smooth-particle simulations of confined free expansions. Gibbs' microcanonical probabilities show that the expansions become truly irreversible as the number of particles is increased. Consider the expansion problem illustrated in the figures. For large N the initial state approaches that of a motionless solid at zero temperature. Classically, such a many-body cold solid state has an entropy of minus infinity. By contrast, the final N-particle state approaches that of a homogeneous fluid, with potential energy Φ equal to one-third the kinetic energy K. Classically, such a many-body hot fluid has a finite entropy $S = Nk \ln[(V/N)(K/N)]$. Evidently the completely time-reversible smooth-particle approximation to the inviscid nonconducting dynamics of an ideal gas introduces a statistical irreversibility even stronger than the kinetic-theory probability ratio of $(1/4)^N$. According to the smooth-particle model, the initial state, which corresponds to a cold motionless crystal from the standpoint of molecular dynamics, has zero measure in the corresponding classical phase space.

Despite this evident change in Gibbs' entropy, Liouville's incompressible theorem [2] guarantees no change in the phase volume occupied by a measurable ensemble of systems undergoing confined free expansion. It seems possible that the true entropy increase could be related to the excess local Kolmogorov entropy (the instantaneous summed positive Lyapunov exponents), with the excess measured relative to the equilibrium Kolmogorov entropy of the final state, but

a check of this conjecture would require a significant computational effort, which we have not yet been able to make.

ACKNOWLEDGMENTS

[1] L. Boltzmann, *Lectures on Gas Theory* [1896,1898], Part I, Sec. 18, translated by S. G. Brush (University of California Press, Berkeley, 1964).

[2] Wm. G. Hoover, J. Chem. Phys. **109**, 4164 (1998).

[3] R. F. Fox, Chaos **8**, 462 (1998).

[4] W. Breymann, T. Tél, and J. Vollmer, Chaos **8**, 396 (1998).

[5] O. Kum and W. G. Hoover, J. Stat. Phys. **76**, 1075 (1994).

[6] L. Lucy, Astron. J. **82**, 1013 (1977).

[7] J. J. Monaghan, Annu. Rev. Astron. Astrophys. **30**, 543 (1992).

[8] W. G. Hoover, T. G. Pierce, C. G. Hoover, J. O. Shugart, C. M. Stein, and A. L. Edwards, Comput. Math. Appl. **28**, 155 (1994).

[9] H. A. Posch and W. G. Hoover, Physica A **240**, 286 (1997).

[10] L. A. Crotzer, G. A. Dilts, C. E. Knapp, K. D. Morris, R. P. Swift, and C. A. Wingate, Los Alamos National Laboratory Report LA-13436-M (April, 1998).

[11] W. G. Hoover, *Computational Statistical Mechanics* (Elsevier, New York, 1991).

[12] J. O. Hinze, *Turbulence* (McGraw-Hill, New York, 1975).

[13] G. K. Batchelor, *An Introduction to Fluid Dynamics* (Cambridge University Press, Oxbridge, England, 1967).

[14] H. A. Posch, Wm. G. Hoover, and O. Kum, Phys. Rev. E **52**, 1711 (1995).

[15] W. G. Hoover and S. Hess, Physica A **231**, 425 (1996).

[16] Wm. G. Hoover and H. A. Posch, Phys. Rev. E **54**, 5142 (1996).

[17] L. D. Landau and E. M. Lifshitz, *Fluid Mechanics* (Addison-Wesley, Reading, MA, 1959).

[18] Wm. G. Hoover, Physica A **260**, 244 (1998).